MAR 26 1998
LIBRARY

UA/PHYS/PET/26-1-98

To appear in the Proceedings of the SPIE's International Symposium
'Medical Imaging 1998', San Diego, California, Feb 21-27, 1998

A Monte Carlo Study of LSO γ-ray Detectors for PET.

G. Tzanakos*, E. Monoyiou, and E. Alexandratou.
University of Athens, Department of Physics,
Division of Nuclear and Particle Physics, Zografou, 15771 Athens, Greece.

UA-PHYS-PET-26-1-98

ABSTRACT

We have made a detailed study of the response of LSO detectors to 511 keV γ-rays. The LSO, discovered recently, has a density greater than BGO, small decay time, and high light output. As such, it should have an overall behavior better than that of BGO. We have modeled a γ-ray detector using an LSO crystal of rectangular cross-section attached to a photomultiplier tube (PMT). We used our PET simulation package to study the energy resolution, efficiency, and timing resolution for various crystal sizes and various energy thresholds. The simulation takes into account the interactions of γ-rays in the crystal via Compton and photoelectric effects, the production and transport of scintillation photons, the productions of photoelectrons in the PMT and the anode signal formation. We have estimated the efficiency versus energy threshold for various lengths of the LSO crystal and we find that for 400 keV threshold this efficiency is large even for 2 cm crystals and comparable to that of BGO. We also estimated the timing resolution (FWHM) versus crystal length for various energy thresholds. The timing resolution is comparable to that of CeF_3 detectors. The energy resolution is about 10 % (FWHM), which allows one to set the energy threshold fairly high.

1. INTRODUCTION

In Positron Emission Tomography (PET) it is important that the basic detector unit is efficient and fast. Efficient detectors require inorganic scintillators with large γ-ray absorption coefficients for photoelectric and Compton interactions at γ-ray energies up to 511 keV. This will ensure that even small crystals can absorb the total energy of the photon, producing signals corresponding to the photopeak values, which can help discriminate against scatter events, without big event losses, leading to efficient count rates and reducing the need for large patient exposures. In addition, the detector should have a fast time response. This will reduce the dead time, allowing smaller exposure times for a given dose or larger number of collected counts for a given time exposure. Thus, an ideal γ-ray detector for PET should be small, to allow for improved spatial resolution, of high density to allow for high efficiency, of high photon yield and small decay time for improved energy and timing resolution. A large number of γ-ray detectors for PET scanners (and also other applications) have been built from NaI, and lately from BGO ($Bi_4Ge_3O_{12}$) [1], as well as in some instances from BaF_2 [2].

Table I: Physical properties of inorganic crystals.

	CeF_3	LSO	NaI	BGO	BaF_2
Density (gr/cm^3)	6.16	7.4	3.67	7.13	4.87
Att. Length (cm)	1.7	1.2	2.9	1.1	2.3
Dec. Constant (nsec)	5, 30	40	230	300	0.6, 620
Peak Emission (nm)	310, 340	420	410	480	225, 310
Index refr.	1.68	1.82	1.85	2.15	1.56
L. O. (ph./MeV)	4400	30000	40000	8200	8500
Hygroscopic	No	No	Yes	No	Slight

Table I shows the physical properties of several inorganic scintillators. Among them, BGO has a large density (allowing for high efficiency), but it also has a long decay time and relatively (compared to NaI) small photon yield, which leads to long dead times and poor timing resolution. On the other hand, BaF_2 has a lower density (being less efficient for comparable size crystals) and it emits light peaking at two wavelengths. One of the two components is very fast (decay constant of 0.6 ns) leading to shorter dead times and better timing resolution.

Fermilab Library
0 1160 0061297 2

A new material, LSO, shortname for Lutetium Oxyorthosilicate ($Lu_2(SiO_4)O$), has been recently discovered [3,4] and small samples have been studied. The physical properties of LSO are listed in Table I. It is clear that LSO has higher density than BGO, a much shorter decay constant (40 ns versus 300 ns) and a four-fold light output (30000 photons/MeV versus 8200 for BGO). Compared to BaF_2 it is also more dense. However, BaF_2 has a much smaller decay time. It is interesting therefore to study the overall response of the LSO and compare with BGO and BaF_2. Due to the fact that only small samples of LSO have been tested, the experimental study of detectors from LSO crystals is not easy. Therefore, we decided to employ our Monte Carlo simulation model [5-8], in order to study the properties of LSO γ-ray detectors. A preliminary study using cylindrical detectors [9] shows a very good performance for small LSO crystals.

2. THE METHOD

For the present study we use a detector model shown in Fig. 1. The detector is made of a rectangular cross section crystal of width a, height b, and length c, attached to a photomultiplier tube (PMT). The signal from the PMT is amplified and driven to the input of a constant fraction discriminator (CFD) as shown in Fig. 1. We use our Monte Carlo package to simulate all

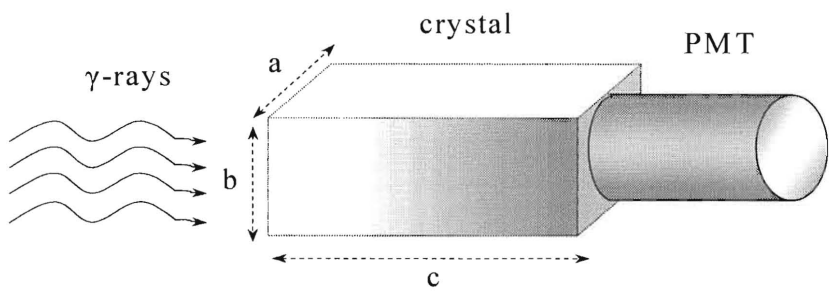

Figure 1. The detector model.

physical mechanisms that contribute to the PMT output signal. This includes the γ-ray interactions inside the crystal, the generation of scintillation photons, the photon transport and the PMT signal formation.

2.1 Interaction of γ-rays

In our model of the γ-ray detector, the front face of the LSO crystal is illuminated perpendicularly and uniformly with γ-rays of 511 keV. Each incident gamma is allowed to interact with the material of the scintillator. There are two possible physical mechanisms: photoelectric absorption and Compton scattering. In the case of photoelectric absorption, the gamma is completely absorbed and no further action is required. In Compton scattering the gamma looses only a fraction of its energy and is allowed to interact again with the material of the scintillator. The algorithm follows each γ-ray until the last interaction is a photoelectric absorption or an escape from the crystal. The probability of occurrence of each interaction depends on the absorption coefficients, μ, of the scintillator, for the two processes. These coefficients were computed from the corresponding total photon cross sections [10] by using the parametrized forms for each kind of atom [11]. These parametrized cross sections have been checked against the cross sections in the nuclear data tables [10]. The absorption coefficients of the scintillator were then calculated by taking into account the atomic composition of the material as follows:

$$\mu = \frac{N_A \rho \sum_i (p_i \sigma(Z_i, E_\gamma))}{\sum_i (p_i A_i)}$$

where: μ: absorption coefficient,
N_A: Avogadro's number
Z_i: atomic number of i-th element of the medium,
A_i :atomic weigh of i-th element of the medium,
ρ: density,
σ: total cross section, and
p_i: proportion by number of the i-th element in the material.

The absorption coefficients computed by this method are shown in Fig. 2 for Compton and photoelectric effects.

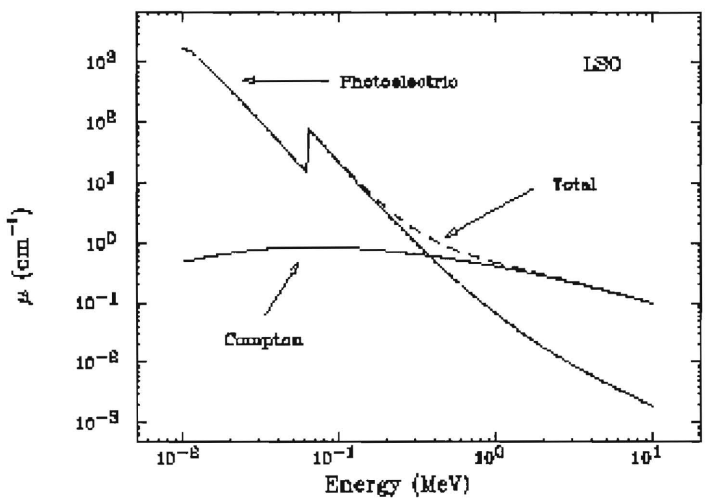

Figure 2: The γ-ray absorption coefficient of LSO for Compton and Photoelectric interactions.

It should be noted here that in Compton scattering the polarization of the incoming and outgoing photons is not modeled. The angular distribution of the scattered photon is given by the Klein Nishina expression [12]:

$$\frac{d\sigma}{d\Omega} = \frac{1}{2} r_0^2 y^2 \left(\frac{1}{y} + y - \sin^2\theta\right)$$

where

$$r_0 = 2.818 \times 10^{-13}\, cm$$

is the classical radius of the electron, and

$$y = \frac{1}{1 + \frac{E}{mc^2}(1 - \cos\theta)} = \frac{E'}{E}$$

is the fraction of the energy that the photon carries after the scattering.

2.2 Photon transport

The energy lost by the γ-ray appears in the form of kinetic energy of produced electrons, and in the form of X-rays in both mechanisms. The electron energy is absorbed by the atoms in the lattice, leading to various excitations and subsequent emission of scintillation photons. We assume that the X-rays are absorbed by the crystal and contribute to the released light in a similar way. The decay time of the excited atoms, the emission spectrum and the light yield depend on the type of the material. Fig. 3

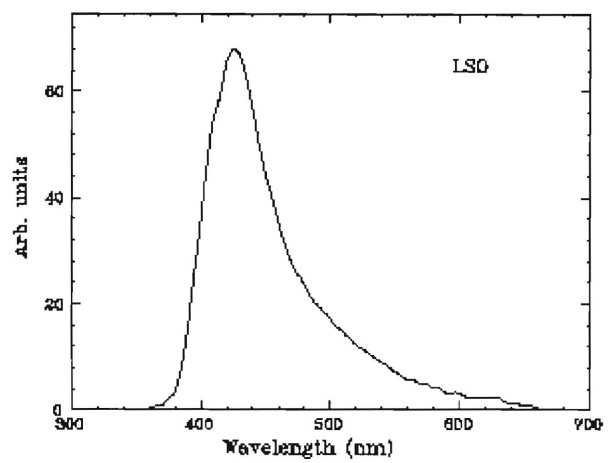

Figure 3. Emission spectrum of LSO.

shows the emission spectrum of the LSO [3,4] according to which we generate scintillation photons. Each photon is transported inside the crystal towards the PMT face following successive reflections on the crystal surfaces, until it reaches the photocathode or escapes due to refraction, provided that it is not absorbed inside the crystal. Various light losses depending on the index of refraction, absorption spectrum and reflectivity of LSO are taken into account. The transmittance has been assumed to be 95% and the crystal reflectivity also 95%. The distribution of arrival times of the scintillation photons, that are produced for each γ-ray, forms the so called cathode illumination function, $I(t)$.

2.3 Signal formation

The distribution $I(t)$ represents the number of photons that reached the photocathode within a given time interval. This time is measured from the moment the γ-ray entered the crystal. The photocathode produces a number of photoelectrons which is determined by its wavelength dependent quantum efficiency. The photoelectrons are then focused towards the first dynode of the PMT. The distribution of their time of arrival is defined as the first dynode illumination function, $I_d(t)$. The function $I_d(t)$ is formed by convolving the photocathode illumination function with the transit time spread (*TTS*) distribution function of the PMT. Then the anode pulse is produced by convolving the function $I_d(t)$ with a function which represents the effect of the PMT's dynodes. Fig. 4 shows the three stages of the signal formation that we just described. It should be noted that the signal decay time is mainly due to the scintillator decay time, not the characteristics of the PMT. The final negative electron pulse is discriminated with a constant fraction discriminator (CFD) in order to produce a timing pulse. We use a CFD instead of a

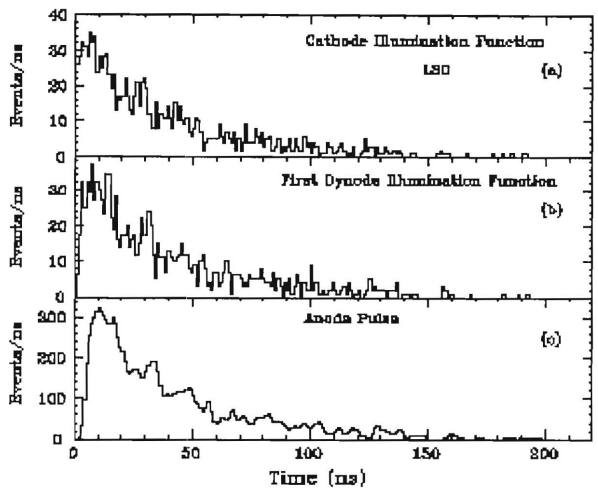

Figure 4. (a) The cathode illumination function, I(t), (b) The first dynode illumination function, $I_d(t)$, (c) The anode current pulse, i(t), for *a*=0.6 cm, *b*=1.2 cm, *c*=2.0 cm.

regular discriminator in order to avoid time slewing due to different size pulses. The energy of the deposited γ-ray is measured by the number of photoelectrons produced at the photocathode, calibrated so that they represent deposited energy. In order to calculate the deposited energy, we assumed that the peak of the distribution of the number of photoelectrons that are produced at the photocathode, for fully absorbed γ-rays, corresponds to 511 keV of detected energy. Fig. 5 shows the distribution of this number for a given crystal geometry (*a*=0.6 cm, *b*=1.2 cm, *c*=4.0 cm).

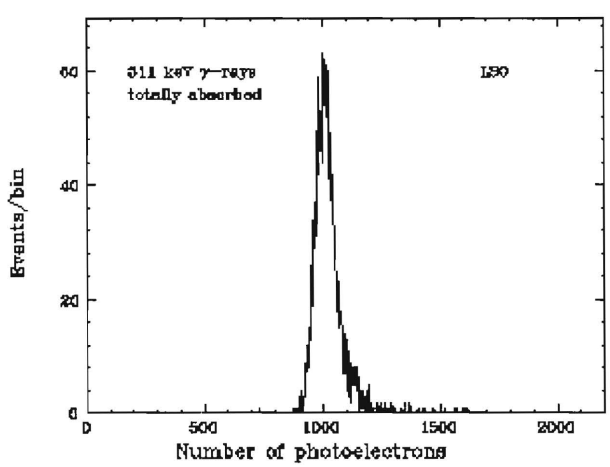

Figure 5. Energy calibration: number of photoelectrons corresponding to 511 keV γ-rays totally absorbed in the crystal.

3. RESULTS

LSO crystals of various dimensions were simulated, and the energy spectra, energy resolution, timing resolution, and efficiency were studied versus crystal dimensions, as well as versus energy threshold. In the simulation, we used a PMT with *TTS* = 2150 ps and rise time = 1250 ps. For each set of dimensions we simulated 5000 incident γ-rays on the front face of the crystal. In Fig. 6 we plot the energy calibration constant versus crystal length. Clearly, wider crystals have more gammas completely absorbed.

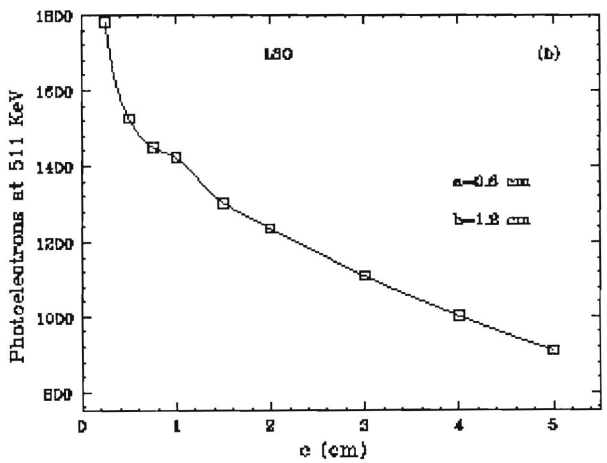

Figure 6. Energy calibration constant versus crystal length.

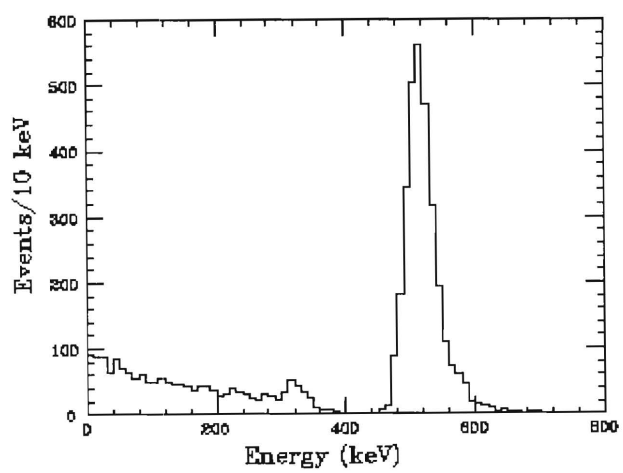

Figure 7. Deposited γ energy (*a*=0.6cm, *b*=1.2 cm, *c*=4.0 cm)

The effect of the length is a little more involving: the longer the crystal, the smaller the effective solid angle. Therefore, the number of collected photoelectrons for fully absorbed γ-rays is smaller.

3.1 Energy resolution

A simulated energy spectrum is shown in Fig. 7. It shows that most of the γ-rays are totally absorbed and only a small percentage undergoes one or more Compton interactions without getting subsequently absorbed. An energy cut (threshold)

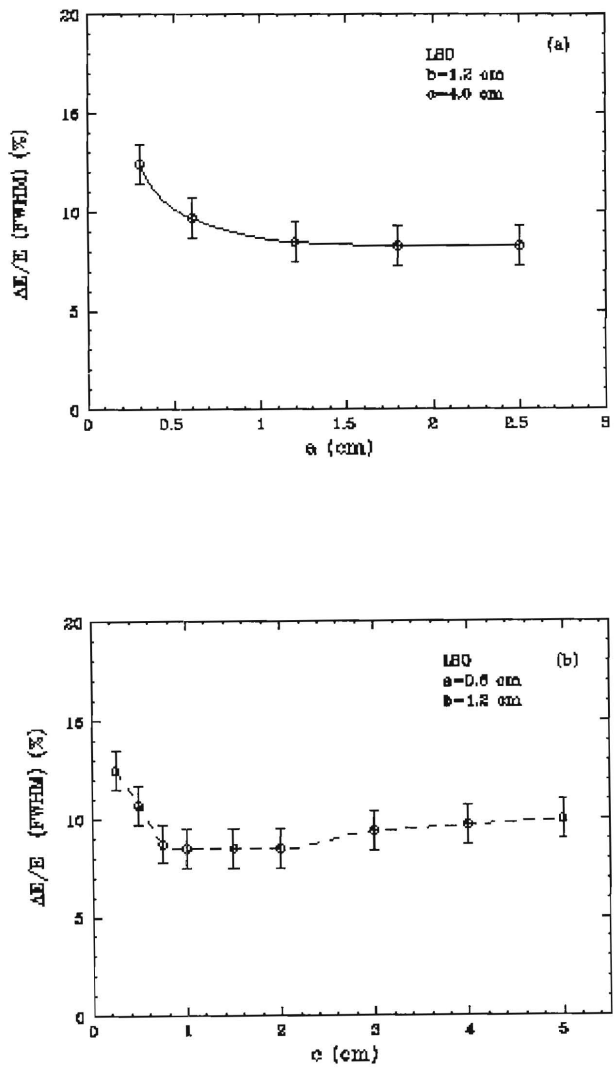

Figure 8. Energy resolution (FWHM) of an LSO detector (a) versus heigth, (b) versus length.

separates clearly the Compton and the photoelectric region. The energy resolution $\Delta E/E$ (FWHM), extracted from this plot, is shown in Fig. 8 as a function of the width, a, and length, c. As a result of the high light output we get a very good energy resolution, which is about 10% at 511 keV. As shown in Fig. 8 the energy resolution is degraded for dimensions smaller than 5 mm.

3.2 Detection Efficiency

We have estimated the efficiency of the detector for various energy thresholds, (E_{cut}) and sizes. The detection efficiency for a given E_{cut} was calculated as the fraction of the incoming γ-rays that are detected, namely those which have an energy deposit E > E_{cut}. Fig. 9 shows the dependence of the detection efficiency on the E_{cut} for various values of the length c, while the other

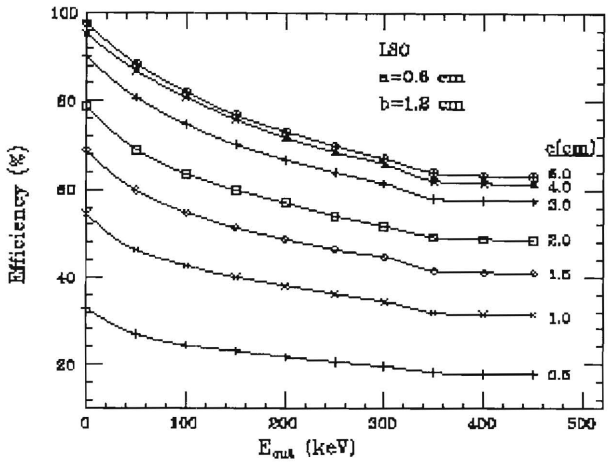

Figure 9. Detection efficiency versus energy threshold.

dimensions are kept fixed at a = 0.6 cm and b = 1.2 cm. We see that for energy thresholds above 200 keV the efficiency is decreasing very slowly with E_{cut} and therefore the choice of E_{cut} is not critical as far as detection efficiency is concerned. The effect of c (length) on the efficiency (for various E_{cut}) is shown in Fig. 10. The rate of increase is small for lengths greater than 3 cm. Therefore, a choice of 3 cm length will be suffice. Fig. 11 shows the dependence of the efficiency on crystal width. The efficiency varies very little for larger widths, however for a very narrow crystal it drops abruptly. For typical crystal sizes, a=0.6 cm, b=1.2 cm the efficiency is good.

3.3 Timing Resolution

In order to study the timing resolution we use the timing pulse from the output of the CFD. We discriminate the analog anode output pulse at 20% of its maximum to form the digital timing pulse. This defines the event time. Using this time, we make a 2-D scatterplot of time versus energy, from which we can form 1-D histograms of time for various energy cuts. A series of such histograms versus E_{cut} is shown in Fig. 12. The tail of the distribution on the side of large times is due to uncertainties associated with small number of photons arriving at the photocathode. This tail disappears and the width of the distribution becomes smaller as E_{cut} becomes larger. The timing resolution, $\Delta\tau$ (FWHM), is extracted from these histograms and plotted versus E_{cut} in Fig. 13. The timing resolution is also plotted versus the dimensions of the crystal in Figs. 14 and 15. These plots show the following characteristics for the timing resolution: (i) $\Delta\tau$ becomes better for higher energy thresholds (ii) it increases linearly with the length of the detector, therefore shorter crystals will have a better resolution and (iii) it decreases (becomes better) with

thicker crystals. The above observations are consistent with the underlying physical mechanisms that are responsible, namely, the variation of possible photon paths, the collection of photons, the decay time of the scintillator and the photon yield. The timing resolution is related to the time slewing of the first detected photon. Thus a short, thick crystal from a material with small decay time and a high photon yield, will produce a phototube signal which when discriminated at high energy threshold will give a timing signal with very little time slewing, in other words very good timing resolution.

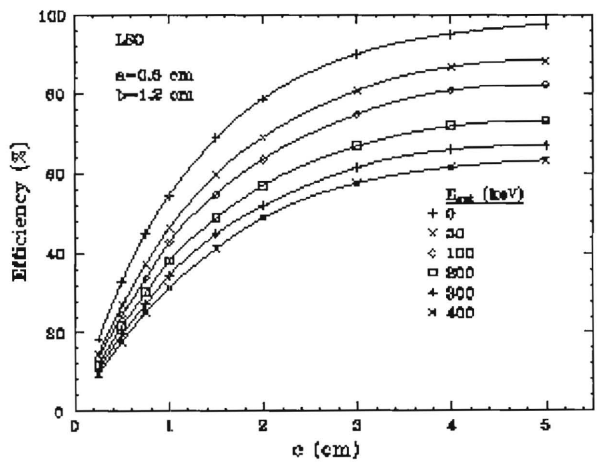

Figure 10. Detection efficiency versus length, for various thresholds.

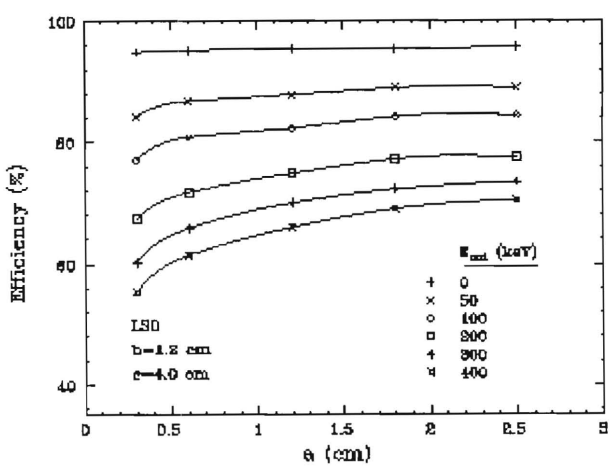

Figure 11. Detection efficiency versus width, for various thresholds.

4. SUMMARY

We have studied the performance of γ-ray detectors from LSO for various sizes and various energy thresholds. We observe that LSO shows very good efficiency, and fairly good timing resolution. For a typical size of 6 mm x 12 mm x 30 mm that is being used in block detectors, we find that for energy threshold at 350 keV the efficiency is 58%. This should be compared to 66% for

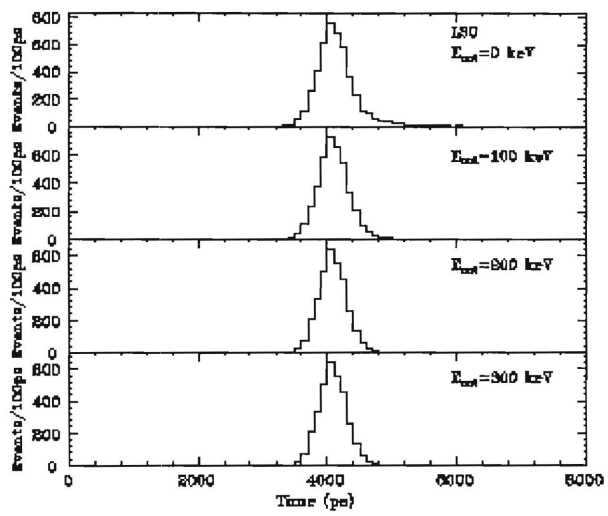

Figure 12. Event time distribution for various energy thresholds. The high tail disappears and the fwhm decreases with increasing energy thresholds.

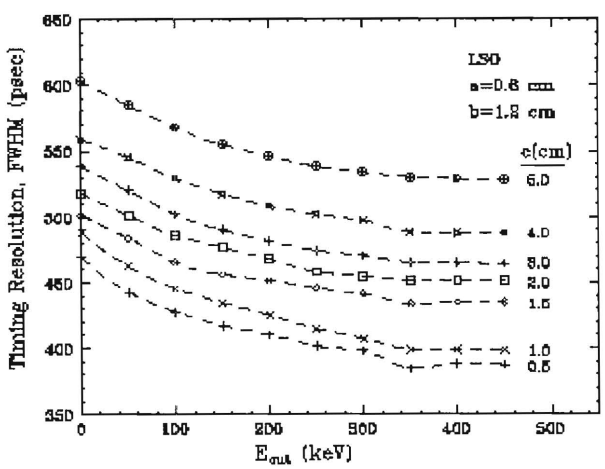

Figure 13. Timing resolution (FWHM) versus energy threshold for detectors of different length.

BGO and 28% for BaF_2. Regarding energy resolution, LSO is the best as compared to other materials. For the typical crystal it is 9.3% at 511 keV. This should be compared to 17% for BGO and 17% for BaF_2. The timing resolution is 465 ps (FWHM). This should be compared to 2070 ps for BGO and 175 ps for BaF_2.

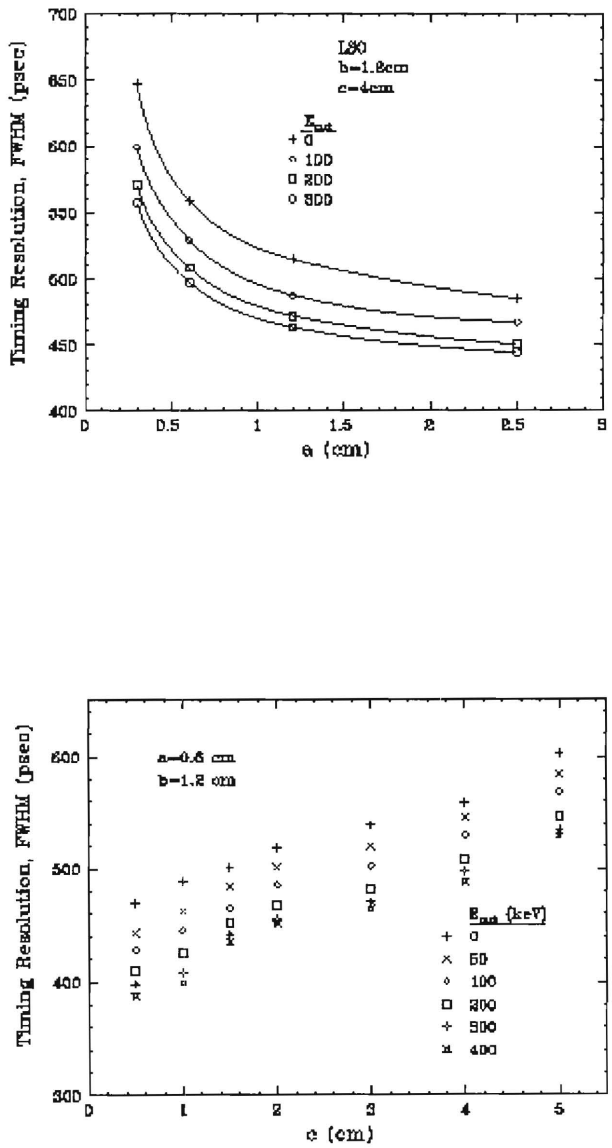

Figure 14. Timing resolution (FWHM) versus detector length.

REFERENCES

- e-mail address: tzanakos@atlas.uoa.gr

1. M.J. Weber and R.R. Monchamp, "Luminescence of $Bi_4Ge_3O_{12}$: Spectral and decay properties", *J. Appl. Phys.*, Vol.44, No. 12, pp. 5495-9, (1973).
2. M. Laval, M. Moszynski, R. Allemand, E.Cormoreche, P. Guinet, R. Ordu, J.Vacher, Barium Fluoride, "Inorganic Scintillator for Subnanosecond Timing, Nuclear Instruments and Methods", *Nuclear Instruments and Methods*, 206, 169, (1983).
3. C. L. Melcher and J.S.Schweitzer, "Cerium-doped Lutetium Oxyorthosilicate" A Fast Efficient New Scintillator, *IEEE Trans. Nucl. Sci.*,Vol.39, No.4, (1992).
4. C.L. Melcher and J.S. Schweitzer, "A promising new scintillator: cerium-doped lutetium oxyorthosilicate", *Nuclear Instruments and Methods in Physics Research A.*
5. G. Tzanakos, M. Bahtia and S. Pavlopoulos, "A Monte Carlo study of the Timing Resolution of BaF_2 for PET", *IEEE Trans. Nucl. Sci.*, 37, 1599 (1990).
6. G. Tzanakos and S. Pavlopoulos, "Development and Validation of a Simulation Model for the Design of a PET scanner", *IEEE Trans. Nucl.Sci.*, 39, 1093-1098, (1992).
7. G. Tzanakos and S. Pavlopoulos, "Design and Performance Evaluation of a New High Resolution Array Module for PET", *1993 IEEE Conference Record, Nuclear Science Symposium and Medical Imaging Conference*, Oct. 30-Nov. 6, 1993, San. Fransisco, CA, p. 1842.
8. S. Pavlopoulos and G. Tzanakos, "Design and Performance Evaluation of a High Resolution Small Animal Positron Tomograph", *1993 IEEE Conference Record, Nuclear Science Symposium and Medical Imaging Conference*, p. 1697 also *IEEE Trans. Nucl. Sci.* TNS, 43, 3249-3255 (1996).
9. G. Tzanakos, Y. Economou, E. Alexandratou, C. Kechribaris, E. Monoyiou and N. Pagoulatos, "A Comparative Study of the Performance Characteristics of New Inorganic Scintillator Detectors for PET", *1995 IEEE Conference Record, Nuclear Science Symposium and Medical Imaging Conference*, Oct. 21-28, San Fransisco, CA.
10. H. Storm, H. I. Israel, Nucl. Data Tables, A7/1970/565
11. A. R. Brun, F. Bruyant, M. Maire, A. C. McPherson, P. Zanarini, GEANT 3, CERN Data Handling Division DD/EE/84-1, 1987
12. O. Klein and Y. Nishina, Z. Physik, 52, 853 (1929)